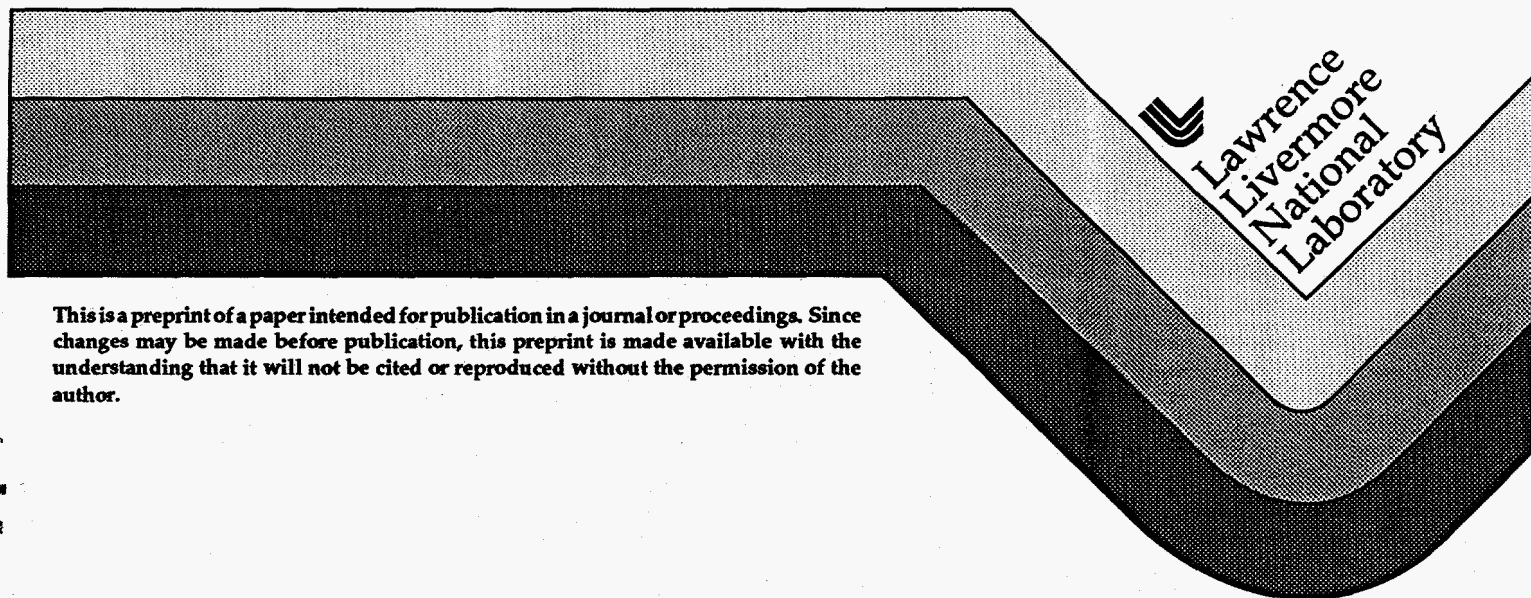# Study of Supra-thermal Electrons and K-α X-rays from High Intensity 500 fs Laser-Produced Plasmas

J. Dunn, B.K.F. Young, A.K. Hankla,
A.D. Conder, W.E. White and R.E. Stewart

Lawrence Livermore National Laboratory

DISCLAIMER

DISCLAIMER

Portions of this document may be illegible in electronic image products. Images are produced from the best available original document.

Study of Supra-thermal Electrons and K-α X-rays from High Intensity 500 fs Laser-Produced Plasmas

J. Dunn, B.K.F. Young, A.K. Hankla,
A.D. Conder, W.E. White and R.E. Stewart

Lawrence Livermore National Laboratory, P.O. Box 808, Livermore, CA 94551 USA

Abstract. We describe recent laser-solid interaction experiments using the 500 fs Janus Nd:glass (1053 nm) laser presently at 1.5 TW power level. The laser beam path is enclosed in vacuum from the compressor to the target and is focused using an off-axis paraboloid. Optical diagnostics monitor the near field pattern, focal spot, spectrum, temporal shape and pre-pulse level. A 12 μm diameter (FWHM) focal spot is achieved (2.5× diffraction limit) corresponding to a peak irradiance of 8×10^{17} W cm^{-2} on target. A suite of x-ray diagnostics characterize the x-ray emission from the plasma. We present results for normal incidence irradiation of high-Z (Zn, Ge, Mo, Sn) solid targets. The supra-thermal electrons produced in the short scale length plasma have temperature T_H >100 keV and can efficiently fluoresce the cold K-α lines in the 8 - 30 keV energy range.

1. INTRODUCTION

The development of compact high power subpicosecond lasers based on chirped pulse amplification (CPA) has introduced a new area of high intensity, ultrashort plasma physics in the last decade (1 - 4). Plasmas of high density and temperature >100 eV are produced when intense ultrashort laser pulses are focused on solid targets (5 - 7). These can be utilized as sources of bright, short lived x-rays from the thermal plasma (7, 8). Experimental work has characterized the absorption (9 - 12) and the production of supra-thermal electrons (12, 13) in the intensity regime of $I \lambda^2 = 10^{15} - 10^{18}$ W cm^{-2} μm^2. Very recently fast electrons from subpicosecond plasmas have been identified as a mechanism for producing short bursts of x-ray continuum and line emission (12, 14 - 16).

In this paper, we describe recent laser-solid interaction experiments with the 500 fs Janus laser at peak irradiances near 10^{18} W cm^{-2} with known laser characteristics. We present results for normal incidence irradiation of high-Z (Zn, Ge, Mo, Sn) targets. The supra-thermal electrons produced in the short scale length plasma have a temperature T_H >100 keV and can efficiently fluoresce cold K-α lines in the hard x-ray 8 - 30 keV energy range.

MASTER

2. JANUS-1ps LASER DESCRIPTION

The Janus-1ps laser has a number of key features: (a) the beam path is enclosed in vacuum from compressor to target; (b) the laser is well characterized for every shot; (c) the laser is integrated into the Janus system allowing the combination of three beams of 500 fs, 100 ps, 1 ns duration for channeling and long scale length pre-formed plasma experiments; (d) an upgrade path to shorter pulses ~250 fs by using mixed silicate/phosphate glass and higher energy ~10 J on target corresponding to $>10^{19}$ W cm^{-2} is available.

The Janus-1ps laser is a hybrid CPA system based on a Ti:Sapphire oscillator and regenerative amplifier front end tuned to 1053 nm wavelength with Nd:phosphate glass power amplifiers. The 100 fs, 1 nJ oscillator output pulse train is stretched to 1.5 ns (FWHM) in a single diffraction grating stretcher: gain narrowing during amplification reduces this to 400 ps. Using polarization rotation, a single chirped pulse is selected and injected into the regenerative amplifier. After multiple passes the pulse is switched out by means of a Pockels cell. It is accompanied by pre-pulses separated by 9 ns corresponding to the cavity's round trip time. A pair of Pockels cells is used to minimize the intensity of these pre-pulses to better than 9 orders of magnitude down from the main pulse. The 1 mJ pulse is amplified using 7 mm, 16 mm and 25 mm diameter rods to ~2 J energy. After amplification, the beam is enlarged to 8 cm diameter and is recompressed in a four grating vacuum compressor to 500 fs. The short pulse beam is relayed under vacuum to the target chamber where it is focused to a 12 μm (FWHM) spot size (2.5× diffraction limit) by a 10 cm diameter off-axis paraboloid with 30 cm focal length. A 5 μm thick nitrocellulose debris shield, protecting the paraboloid, is the only post compression transmissive optic, thus minimizing self-focusing effects. The throughput loss due to the compressor and optics after the final
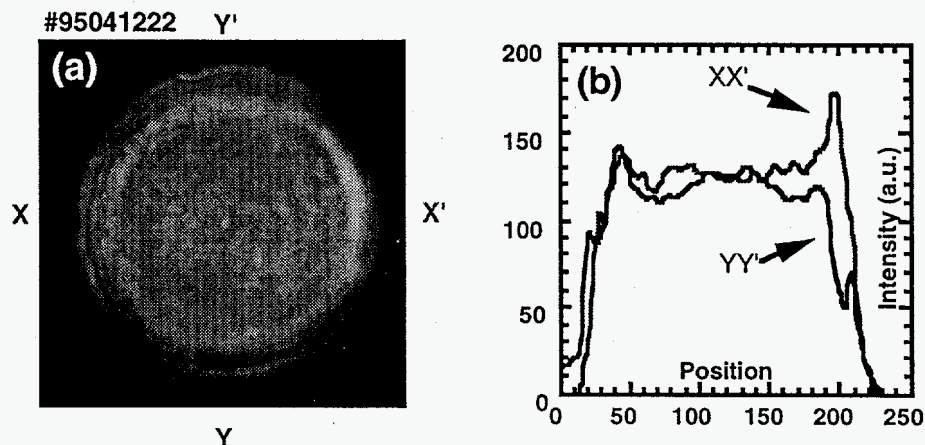

FIGURE 1. (a) Near field beam image at full power is measured by CCD camera. (b) Lineout showing good flat top profile across the beam diameter.

amplification stage results in a maximum of 700 mJ energy on target. With the temporal and focus shape described below, this laser energy corresponds to a peak irradiance of 8×10^{17} W cm^{-2}. The laser can be fired at a repetition rate of 1 shot every 3 minutes and the energy is repeatable to within ± 5%.

Laser parameters including energy, temporal shape, pre-pulse, near field image, focal spot and spectrum are monitored on every shot. The near field beam pattern is recorded by a charge-coupled device (CCD) camera system. Figure 1 shows a typical flat top profile measured at full power after the 25 mm rod. After amplification and appropriate attenuation, the laser focus from the paraboloid is imaged with an f/2 microscope objective with 2μm resolution onto an IR calibrated CCD camera. Figure 2 (a) and (b) show the image and lineout of the 12.6×13.0 μm^2 (FWHM) focus spot measured at full power.
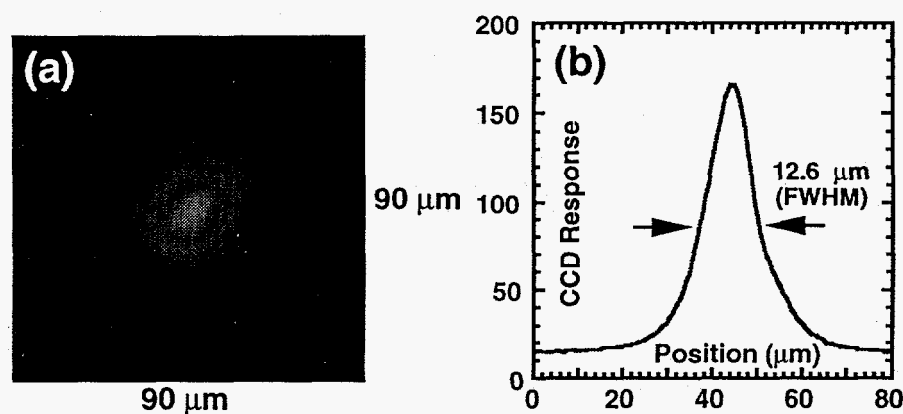
FIGURE 2. (a) Image and (b) lineout of the laser focus spot (12.6×13.0 μm^2 (FWHM)) measured at full power.
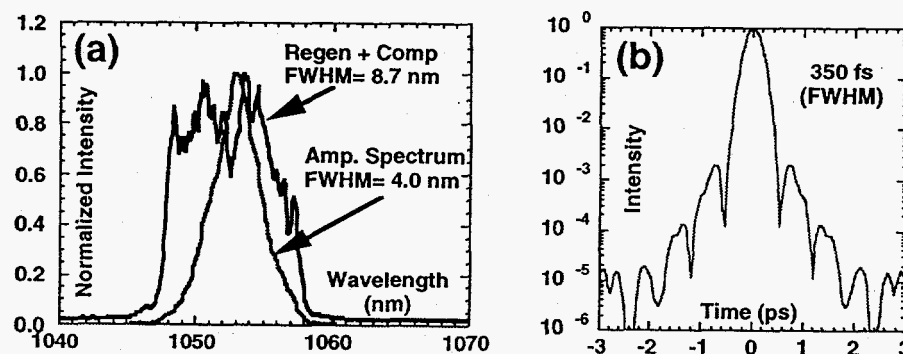
FIGURE 3. (a) Spectrum of the regenerative amplifier beam after the compressor and at full power. (b) Semi-logarithmic plot showing expected pulse shape obtained from the Fourier transform of the laser spectrum taken at full power.

The laser spectrum is monitored at the stretcher and compressor. Figure 3 (a), shows the spectrum at 1053 nm for the regenerative amplifier beam after the compressor with a measured bandwidth of 8.7 nm (FWHM). For full system

power shots, 4.0 nm (FWHM) is measured after the compressor: this is sufficient bandwidth to support 400 - 500 fs (FWHM) pulse widths. Figure 3. (b) is a semi-logarithmic plot showing the expected laser pulse shape obtained by taking the Fourier transform of the spectrum after the compressor at full power. The central feature best fits a *sech*^{2} function with a 350 fs (FWHM). The finite size of the gratings results in spectral clipping of the diffracted beam during compression: this introduces a *pedestal* on the main pulse at a level 2×10^{-3}, 10^{-4}, 10^{-5} of the peak intensity for -0.7 ps, -1.4 ps, -2.2 ps, respectively.
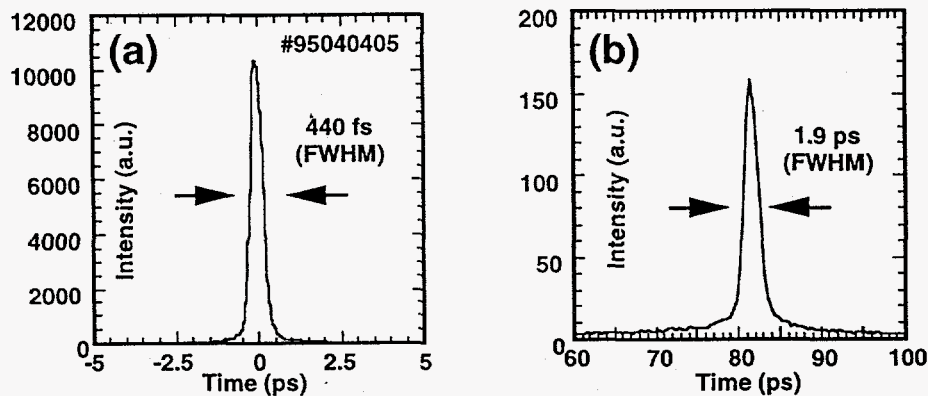

FIGURE 4. (a) Pulse width of 440 fs (FWHM) is measured using a second order single shot autocorrelator, and (b) 1.9 ps instrument limited width from optical streak camera.

The temporal shape and *pre-pulse* are studied as follows. A calibrated second order single shot autocorrelator with 10^4 dynamic range in a 6 ps time window measures the pulse after compression; Figure 4 (a) shows a 440 fs (FWHM) laser pulse at full power. A third order scanning autocorrelator with more dynamic range has measured the laser pulse and confirmed the pedestal of Figure 3 (b). A Hamamatsu C1587 optical streak camera is used to study the 2 ps to 1 ns time frame. The intensifier readout is lens-coupled to a 16-bit CCD camera (17) giving 10^2 - 10^3 dynamic range relative to the intensifier noise floor. Figure 4 (b) shows a measured width of 1.9 ps (FWHM) from the streaked image: although limited by the streak camera instrumental resolution (> 1.3 ps) this is in agreement with Figure 4 (a). A fast calibrated photo-diode monitors back reflected laser energy from the target and can detect the presence of a pre-pulse 9 ns before the main pulse due to leakage from the the regenerative amplifier. At full power, this pre-pulse level is measured to be $< 3 \times 10^{-10}$ of peak intensity.

3. EXPERIMENTAL DESCRIPTION AND RESULTS

A suite of x-ray instruments have characterized the spatial, spectral and temporal characteristics of the x-ray emission from the high intensity laser-produced plasma. These include x-ray sensitive CCD cameras, a 7-channel

filtered NaI scintillator array, a pin diode array, a modified Kentech x-ray streak camera with 2 ps time resolution and various crystal spectrometers. We describe initial results for high-Z slabs where the target is irradiated at *normal incidence* to the laser axis. The 15× magnification x-ray sensitive CCD pinhole camera, described in (18), has 5 - 15 μm diameter apertures positioned ~15 mm from the plasma and filtered with 25 μm Be. The CCD readout allows immediate access to time integrated soft 0.8 - 8 keV x-ray images of the laser spot. Optimum focusing of the laser can be be found in a few shots. It also provides spatial information of the laser intensity for accurate determination of the irradiance parameter. Figure 5 (a) is a profile plot of the soft x-ray image emitted from a Ge slab irradiated with 370 mJ energy at near best focus at 2×10^{17} W cm^{-2}. The measured 14.4 μm (FWHM) from the x-ray spot size is in close agreement with the laser optical focus images recorded at high power, see Figure 2. Spectra recorded simultaneously show that the 8 - 10 Å Ne- and Na-like n = 3 - 2 Ge lines are the brightest x-ray features. High Z targets e.g. Ge ionized to the L-shell are observed to generally radiate stronger 1 - 3 keV x-rays than K-shell ionized Al. Detectable x-ray images can be recorded for >50 mJ laser energy on a Ge slab.

The CCD has excellent linearity between x-ray energy and electron-hole pair production, requiring 3.65 eV x-ray energy/ electron-hole pair (19, 20). When low noise CCDs are cooled, this inherent energy dispersive characteristic combined with high quantum detection efficiency (>50% at 4 keV) and good 2-dimensional spatial resolution (<25 μm) allows the detection and discrimination of single x-ray photons (0.5 - 20 keV). For these reasons, the CCD detector has been utilized extensively by the astrophysical community. It has recently been applied to 3 mJ, 100 fs laser-plasmas (15, 16). We use a 1024 × 1024 pixels CCD camera cooled to -35°C (17) with low read noise 8 electrons rms. and dark current measured at 0.5 electron pixel^{-1} s^{-1}. With a pixel full well capacity of 250 k electrons this gives excellent 15-bit dynamic range. The pulse height spectrum of known K-α lines self-calibrates the detector energy response and agrees with the optical calibration of linearity to better than 0.7%. An algorithm is used to look for charge in isolated pixels produced by x-rays absorbed in the depletion region of the detector.

The CCD detector was placed 93 cm from the plasma at 15° from the target normal. A filter array of 50 μm Cu, 50 μm Y, 50 μm Nb, 50 μm Ta was mounted in a nose cone ~12 cm from the CCD detection plane to provide different energy channels. No fluorescence of the array was observed during the experiment. The photon flux, mainly continuum emission, in the x-ray channels below 8 keV was significantly high to make detection of single photon events difficult for laser energies >100 mJ. Therefore, target materials of Zn with 8.63 keV K-α and higher were studied. At $\sim 10^{18}$ W cm^{-2}, energetic events identified as 50 - 200 keV continuum x-rays could be detected uniformly across the CCD. The NaI scintillator array measured supra-thermal electron temperatures $T_H > 100$ keV.

Figure 5 (b) indicates the observed x-ray pulse height spectrum for single pixel events from a 25 μm thick Mo foil irradiated at full power. The Mo K-α and K-β fluorescence lines at 17.5, 19.6 keV, respectively, are labelled. The background between 5 - 20 keV is mainly due to continuum x-rays but may include partial events from the Mo K-α line. The peak at 1.5 keV is a combination of thermal noise and partial events. The CCD energy resolution of 210 eV (FWHM) at ~17.5 keV, determined from (19), gives $E/\Delta E \sim 80$ for the detector.

The focus spot was made slightly larger by moving the target towards the paraboloid by 200 μm into the converging laser beam. The laser energy was varied from 20 to 600 mJ corresponding to $5 \times 10^{15} - 2 \times 10^{17}$ W cm^{-2} while the focus remained constant. Figure 5 (c) shows the dependence of the 17.5 keV Mo K-α fluorescence as a function of laser energy. There are a number of interesting features. The K-α fluorescence is observed to scale linearly with the laser energy and the conversion efficiency remains constant over nearly 2 orders of magnitude laser intensity. Secondly, at low intensity the K-α fluorescence is still generated efficiently which indicates a hot electron temperature $T_H \sim 20$ keV.
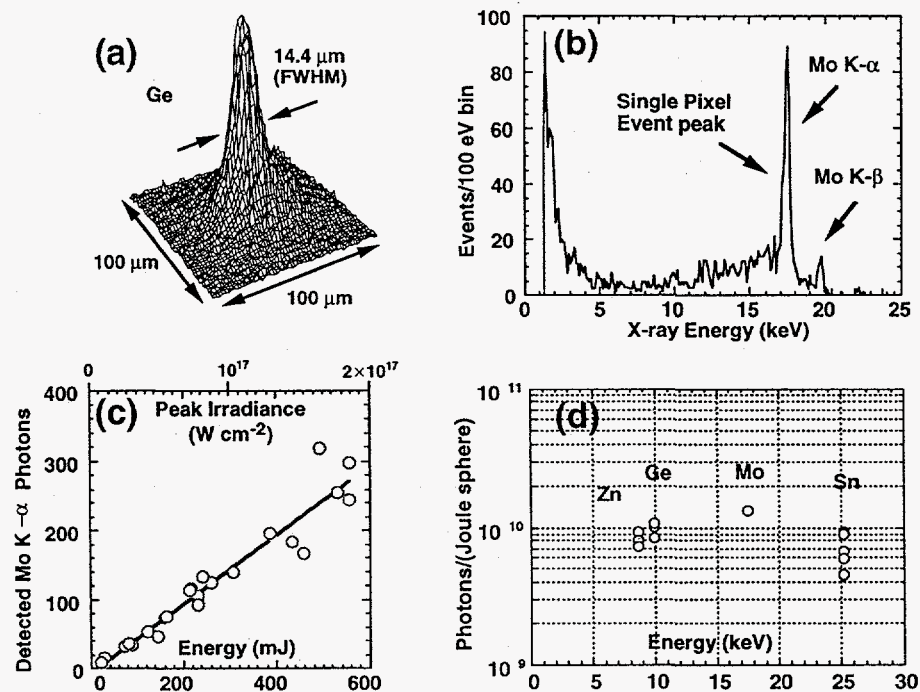

FIGURE 5. (a) Soft x-ray image of the plasma produced by irradiating an optically polished Ge slab with 370 mJ energy at best focus. The focal spot size is 14.4μm (FWHM). (b) Pulse height spectrum showing intense Mo K-α and K-β fluorescence lines at 17.5, 19.6 keV, respectively from laser heated Mo target. (c) Detected Mo K-α photons as a function of laser energy from 20 mJ to 600 mJ. (d) K-α yield measured at high intensity 5×10^{17} W cm^{-2}. (The two lowest Sn data points are at 2×10^{17} W cm^{-2}).

Figure 5 (d) shows the measured K-α yield for different targets at best focus ~5×10^{17} W cm^{-2} and normal incidence. The measured K-α yield takes account of the CCD quantum detection efficiency for the depletion region thickness, the filter response and the solid angle, assuming isotropic x-ray emission. Yields of >10^{10} photons /(Joule sphere) are measured for all target materials.

4. DISCUSSION AND CONCLUSIONS

The role of the amplified spontaneous emission (ASE) pedestal of the laser pulse has been discussed for 100 fs experiments (14 - 16). An ASE pedestal 2 ns before the main pulse and at 10^{-6} lower intensity has been reported as necessary for the efficient production of energetic x-rays >20 keV for ~10^{18} W cm^{-2} intensities (14). Similarly, it has been noted at 3×10^{16} W cm^{-2} that a controlled ASE pedestal enhances the hot electron conversion efficiency and 1.5 - 6.4 keV K-α fluorescence production (15, 16). The intensity of the pedestal is close to the damage threshold of the target material (15) and rippling of the target surface by the ASE is a possible explanation for this phenomena; higher thermal x-ray emission has also been seen for 100 fs irradiation of textured surfaces (8).

In comparison, this experiment at 500 fs, 1053 nm at near 10^{18} W cm^{-2}, has a pre-pulse level ~10^9 W cm^{-2} which is close to or below the expected target damage. If a *pre-pulse* arriving nanoseconds before the main pulse has an effect on hot electron generation and x-ray production, then some change in the K-α emission would be noted as the laser intensity is reduced. This is not observed in Figure 5 (c) which exhibits a linear scaling of the K-α yield with laser energy down to 5×10^{15} W cm^{-2}. Differences in the temporal shapes of the pulses may be part of the explanation. The 500 fs laser pulse is 4× longer and has a significant *pedestal* intensity 3 - 5 ps before the peak of the pulse, see Figure 3 (b). This would pre-form a short scalelength plasma and establish a critical density surface before the peak of the pulse. Significant absorption into hot electrons is observed as inferred by the K-α emission for the 500 fs pulses. The details of the laser absorption mechanism at normal incidence is beyond the scope of this discussion.

Table 1, on next page, shows the absolute 8 - 25 keV K-α conversion efficiency for the studied targets: Mo and Sn have a maximum of ~4×10^{-5} of the incident laser energy converted into 17.5 and 25.2 keV monochromatic x-rays. Zn and Ge have a 50% lower value. Studies of high intensity 100 fs experiments (16) observe hot electron pumped 1.5 - 6.4 keV K-α fluorescence for Al, Ca, Fe targets with 12% absorption into 8 keV hot electrons. Quoted conversion efficiencies of ~8×10^{-5} for 6.4 keV x-rays are higher than reported here. This slightly higher conversion at lower x-ray energies may be explained by additional pumping from the tail of the thermal electron distribution.

In conclusion, we have shown that high intensity 500 fs laser plasmas can be used as an intense source of hard, 8 - 30 keV, monochromatic x-rays.

Table 1. K-α X-ray Conversion Efficiency

Z	Element	E (keV)	Conversion efficiency into K-α
30	Zinc	8.63	1.3×10^{-5}
32	Germanium	9.88	1.7×10^{-5}
42	Molybdenum	17.5	3.7×10^{-5}
50	Tin	25.2	3.7×10^{-5}

ACKNOWLEDGMENTS

REFERENCES

1. Strickland, D., and Mourou, G., *Opt. Commun.* **56**, 219 (1985).
2. Milchberg, H. M., et al, *Phys. Rev. Lett.* **61**, 2364 (1988).
3. Kieffer, J. C., et al, *Phys. Rev. Lett.* **62**, 760 (1989).
4. Murnane, M. M., Kapleyn, H. C., and Falcone, R. W., *Phys. Rev. Lett.* **62**, 155 (1989).
5. Cobble, J. A., et al, *Phys. Rev. A.* **39**, 454 (1989).
6. Audebert, P., et al, *Europhys. Lett.* **19**, 189 (1992).
7. Kieffer, J. C., et al, *Phys. Fluids B* **5**, 2330 (1993).
8. Gordon, S. P., et al, *Opt. Lett.* **19**, 7 (1994).
9. Fedosejevs, R., et al, *Appl. Phys. B* **50**, 79 (1990).
10. Klem, D. E., Darrow, C., Lane, S., and Perry, M. D., in *Proceedings of Short-Pulse High-Intensity Lasers and Applications II SPIE Vol.* **1860**, 1993, pp. 98.
11. More, R. M., et al, these proceedings (1995).
12. Nickles, P. V., et al, these proceedings (1995).
13. Darrow, C., Lane, S., Klem, D. E., and Perry, M. D., in *Proceedings of Short-Pulse High-Intensity Lasers and Applications II SPIE Vol.* **1860**, 1993, pp. 46.
14 Kmetec, J. D., et al, *Phys. Rev. Lett.* **68**, 1527 (1992).
15. Rousse, A., et al, *J. Phys. B: At. Mol. Opt. Phys.* **27**, L697 (1994).
16. Rousse, A., et al, *Phys. Rev. E* **50**, 2200 (1994).
17. Conder, A. D., Dunn, J., and Young, B. K. F., *Rev. Sci. Instrum.* **66** (1) 709 (1995).
18. Dunn, J., Young, B. K. F, and Shiromizu, S. J., *Rev. Sci. Instrum.* **66** (1) 706 (1995).
19. Lumb, D. H., and Hopkinson, G. R., *Nucl. Instrum. Methods* **216** 431 (1983).
20. Lumb, D. H., and Holland, A. D., *Nucl. Instrum. Methods* A**273** 696 (1988).